


# **An Analysis of the Effects of Isocurvature Fluctuations in Dantes Inferno Multi-Field Inflation Models**

A thesis submitted in partial fulfillment of the requirement  
for the degree of Bachelor of Science with Honors in  
Physics from the College of William and Mary in Virginia,

by

Brandon M. Buncher

Accepted for Honors 



Advisor: Prof. Joshua Erlich

  
Gina L. Hoatson

Prof. Gina L. Hoatson



Prof. Jun-Ping Shi

Williamsburg, Virginia  
May 2017

# Contents

<b>Acknowledgments</b>	<b>ii</b>
<b>Abstract</b>	<b>v</b>
<b>1 Introduction</b>	<b>1</b>
1.1 Motivation and Goals . . . . .	1
<b>2 Theory</b>	<b>2</b>
2.1 General Relativity . . . . .	2
2.2 The Cosmic Microwave Background . . . . .	4
2.3 Single-Field Models of Inflation . . . . .	6
2.4 Multi-Field Models of Inflation . . . . .	9
2.5 Outline . . . . .	12
<b>3 Procedure and Results</b>	<b>13</b>
3.1 Single-Field Models of Inflation . . . . .	13
3.2 Multi-Field Models of Inflation . . . . .	15
3.3 Dante's Inferno . . . . .	18
3.3.1 Numerical Results . . . . .	20
3.4 Conclusions and Future Plans . . . . .	25

# Acknowledgments

I would like to thank Dr. Joshua Erlich for his immense help and support in completing this project. In addition, I owe great appreciation to Dr. Carl Carlson for his excellent mentorship throughout my college experience. Finally, I would like to thank the entire physics department at the College of William and Mary for a phenomenal undergraduate experience.

## **Abstract**

Although there is significant evidence of inflation (a period of rapid expansion of the early universe), a definitive model of the epoch has not yet been widely accepted. A variety of models exist which describe this period; however, current technology cannot adequately measure several key factors that would demonstrate the veracity of these models. A major differentiator between classes of models is the number of fields that contribute to the inflationary epoch. Single-field inflation models assume the existence of a single field, though the details of this field vary depending on the model, while multi-field inflation models assume the existence of two or more fields. In this project, we study a class of multi-field models in order to determine the magnitude of isocurvature fluctuations, which have been assumed negligible in previous studies.

# Chapter 1

## Introduction

### 1.1 Motivation and Goals

The data obtained by the Planck satellite indicates that isocurvature field fluctuation modes were suppressed during inflation, while adiabatic fluctuations were not. In general, models of inflation do not inherently suppress these modes, so it is a requirement for inflationary model to naturally lack these fluctuations. In various spiral inflation models, such as Dante's Inferno, it has previously been assumed [1] [2] [3] that isocurvature fluctuations are negligible; however, this is not a trivial assumption. In this paper, we demonstrate that the isocurvature modes are negligible in the Dante's Inferno model of inflation, support this conclusion using numerical calculations, and generate predictions of the Dante's Inferno model.

In this report, the speed of light and Newton's gravitational constant are defined as  $c = 1$  and  $G = 1$ , respectively. In addition, the metric signature  $(-1, 1, 1, 1)$  is used.

# Chapter 2

## Theory

### 2.1 General Relativity

As described by Einstein's theory of general relativity, the effects of gravity may be attributed to the curvature of spacetime. Information of this curvature is stored in the spacetime metric  $g_{\mu\nu}$ , a four-dimensional symmetric tensor [4] [5]. Here,  $\mu$  and  $\nu$  may take on the values 0, 1, 2, or 3. 0 describes time, while 1, 2, and 3 describe space. Terms with lower indices are covariant quantities. Under the change of coordinates  $x_\mu \rightarrow x'_\mu$ , an arbitrary covariant vector  $A_\mu$  transforms as  $A_\mu \rightarrow A'_\mu = \frac{\partial x^\nu}{\partial x'^\mu} A_\nu$ . Conversely, under the change of coordinates  $x^\mu \rightarrow x'^\mu$ , an arbitrary contravariant vector  $A^\mu$  transforms as  $A^\mu \rightarrow A'^\mu = \frac{\partial x'^\mu}{\partial x^\nu} A^\nu$ . Contravariant vectors such as velocity are indicated with an upper index. Indices may be lowered and raised using the spacetime metric  $g_{\mu\nu}$  and inverse spacetime metric  $g^{\mu\nu}$  respectively, which possess the property  $g_{\mu\alpha} g^{\alpha\nu} = \delta_\mu^\nu$ , where  $\delta_\mu^\nu$  is the Kronecker delta function. Repeated indices are summed over.

The metric  $g_{\mu\nu}$  is a two index tensor, and may be interpreted as a four-by-four matrix, where  $\mu$  and  $\nu$  denote the row and column number, respectively. In flat spacetime,

$g_{\mu\nu} = \eta_{\mu\nu} = \begin{pmatrix} -1 & 0 & 0 & 0 \\ 0 & 1 & 0 & 0 \\ 0 & 0 & 1 & 0 \\ 0 & 0 & 0 & 1 \end{pmatrix}$ , the Minkowski metric. A metric may be described by a line element  $ds^2$ ; for the Minkowski metric,  $ds^2 = -dt^2 + dx_i dx^i$ . The line element is a generalization of the Euclidean line element  $ds^2 = dx^2 + dy^2 + dz^2$ , and describes the length of an infinitesimal displacement in space and time [4] [5].

The Minkowski metric is valid exactly only in flat spacetime, though may be used to approximate spacetime with slight curvature. As the universe exhibits little net curvature over large scales, the Minkowski metric provides an accurate characterization; however, the Minkowski metric fails to describe the effects of inflation [5]. Though the inflationary epoch has ended, spacetime continues to expand at an accelerating rate due to the presence of dark energy. As a result, the distance between two points in space increases as time progresses, indicating that the static Minkowski metric is insufficient when describing inflating spacetime. The comoving coordinates provide a set of coordinates consistent throughout time by through the inclusion of the scale factor  $a(t)$ , a dimensionless function of time which accounts for the inflation of spacetime [5]. Through the inclusion of the scale factor, the Minkowski metric may be altered to produce the Friedmann-Lemaître-Robertson-Walker (FLRW) metric

$$g_{\mu\nu} = \begin{pmatrix} -1 & 0 & 0 & 0 \\ 0 & a^2 & 0 & 0 \\ 0 & 0 & a^2 & 0 \\ 0 & 0 & 0 & a^2 \end{pmatrix}, \quad (2.1)$$

with the line element  $ds^2 = -dt^2 + a^2 dx_i dx^i$ . This metric accounts for inflation by parameterizing spacetime in terms of the comoving distance [5].

## 2.2 The Cosmic Microwave Background

Measurements of a cosmic observable may correlate with one another when the measurement locations are spatially close; however, observations at distant locations exhibit little correlation. The degree of correlation may be quantified through a correlation function: for an observable  $R$ , the correlation between measurements of  $R$  at the locations  $\vec{x}$  and at  $\vec{y}$  is defined as  $\langle R(\vec{x})R(\vec{y}) \rangle$ . A measurement of  $\langle R(\vec{x})R(\vec{y}) \rangle = 0$  implies that there is no correlation between  $R(\vec{x})$  and  $R(\vec{y})$ , indicating that they are not causally connected. Correlation functions may be generalized to describe the correlation between observables at an arbitrary number of locations, though it is assumed that only two-point correlation functions are non-negligible [5].

By taking the Fourier transform of a correlation function, the power function  $P(k)$  may be created. Observations indicate that the initial density power spectrum (which maps to the initial temperature power spectrum) should exhibit approximate scale invariance, taking the form of  $P(k) \propto k^{n_s-1}$  [6].  $n_s$  is the scalar tilt, which represents the deviation of the power spectrum from exact scale invariance and is defined as  $n_s - 1 = \frac{d \ln P(k)}{d \ln k}$  [5].

The cosmic microwave background (CMB) describes the 2.7 K background radiation resulting from the Big Bang. As a result of inflation, areas that currently are now of adequate distance from one another to preclude interaction may have once been correlated. Thus, temperature correlation functions relating distant locations in space may be non-zero, as the locations may have had causal contact at an earlier time. The density correlation function (which maps to the temperature correlation function) between two points may be expressed



in terms of spherical harmonics as

$$\langle T(\theta, \phi) T(\vec{0}) \rangle = \sum_m c_m Y_{\ell m}(\theta, \phi), \quad (2.2)$$

where  $c_m$  are real numbers and  $\vec{0}$  represents the origin from which  $\theta$  and  $\phi$  are defined [5]. From this expression, the correlation function may be decomposed in terms of spherical harmonics as

$$P_\ell = \sum_m |c_{\ell m}|^2, \quad (2.3)$$

where

$$c_{\ell m} = \frac{i^\ell k}{(2\pi)^{3/2}} \int T(\vec{k}) Y_{\ell m}^*(\hat{k}) \sin \theta d\theta d\phi, \quad (2.4)$$

where  $Y_{\ell m}^*(\hat{k})$  indicates the complex conjugate of the spherical harmonic function  $Y_{\ell m}$ . By propagating the initial power spectrum forward in time using a transfer function, the power spectrum displayed in Figure 2.1 may be created, which shows CMB temperature fluctuations as a function of angular scale [7]. In this figure, the observed temperature fluctuations correspond remarkably well with the theoretical predictions assuming a scale invariant initial power spectrum (a power spectrum that does not exhibit different behavior at different dimensionful scales), providing support for the theory of inflation [8]; however, the existence of a scale invariant initial power spectrum does not solely imply inflation [9].

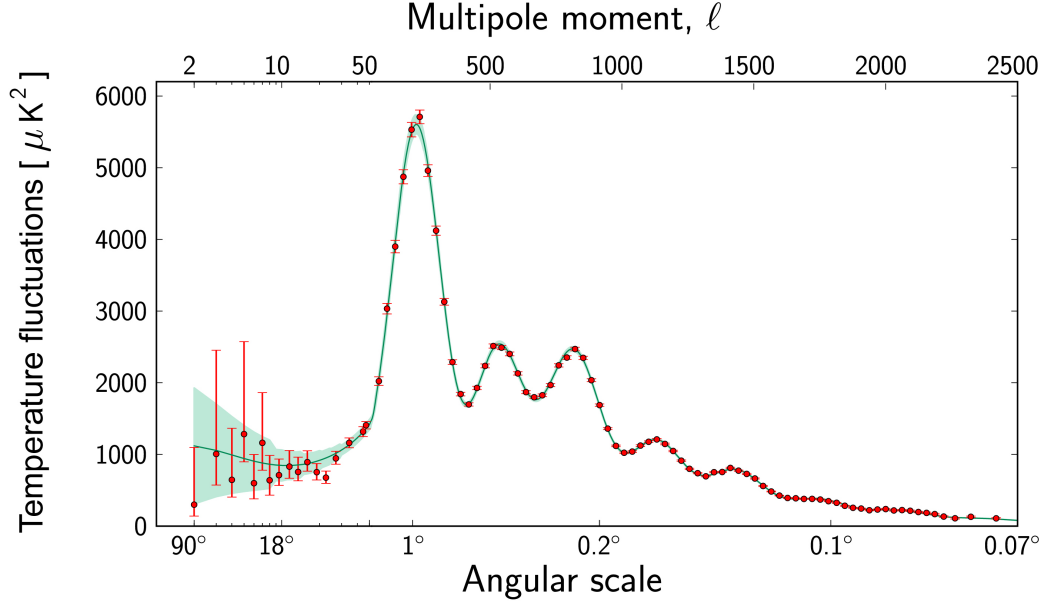


Figure 2.1: The power spectrum  $P_\ell$  as a function of angular scale. The solid green line and shaded area correspond to the theoretical prediction and error of  $P_\ell$ , while the red points (together with error bars) correspond to the initial power spectrum that, when propagated forward in time, creates the temperature fluctuations observed today. The extremely high degree of agreement between prediction and observation provide support for a nearly scale invariant initial power spectrum such as inflation [7].

## 2.3 Single-Field Models of Inflation

Single-field models of inflation assume the existence of a single field that produced the exponential increase in spatial volume of the early universe. These models typically utilize a scalar inflaton field that exerts a negative pressure [5]. This field is predicted to have existed at an unstable state when the Big Bang occurred, and in the moments after, rapidly transitioned to a lower energy state, triggering the exponential expansion of spacetime characteristic of the inflationary epoch [5]. During the inflationary period, which began roughly one Planck second after the Big Bang and lasted  $10^{-33}$  s, spacetime increased in radius by

a factor of around  $10^{26}$  [5]. A general form of the Lagrangian describing this field is

$$\mathcal{L} = \partial_\mu \phi \partial^\mu \phi - V(\phi), \quad (2.5)$$

where  $\phi$  is the scalar inflaton field and  $V(\phi)$  represents the unique potential describing a given inflaton field [8] [9]. Here,  $\partial_\mu$  and  $\partial^\mu$  represent derivatives with respect to the contravariant coordinate  $x^\mu$  and the covariant coordinate  $x_\mu$ , respectively. The equations of motion for a scalar field may be found by varying the action  $\int \mathcal{L} d^3x$  [5]:

$$\frac{1}{\sqrt{-g}} \partial_\mu \left( \sqrt{-g} g^{\mu\nu} \partial_\nu \phi \right) = - \frac{\partial V(\phi)}{\partial \phi}. \quad (2.6)$$

Here,  $g^{\mu\nu}$  represents the inverse spacetime metric, and the scalar  $g$  represents the determinant of this metric. These equations, when solved, provide a description of the behavior of the field  $\phi$  as a function of time, allowing the calculation of inflationary observables such as  $n_s$ .

The major differentiator between scalar single-field models of inflation is the potential  $V(\phi)$ . The potential may take on many forms; for example, for a massive scalar field,

$$V(\phi) = \frac{1}{2} m^2 \phi^2, \quad (2.7)$$

where  $m$  represents the mass of the field [5]. In Minkowski spacetime, the equations of motion derived from this potential take on the form of the familiar Klein-Gordon equation [5],

$$\partial_\mu \partial^\mu \phi + m^2 \phi = 0; \quad (2.8)$$

however, numerous models of inflation utilize the FLRW metric, which corresponds to the line element [5] [9]

$$ds^2 = -dt^2 + a^2 dx_i dx^i. \quad (2.9)$$

In this spacetime geometry,  $\sqrt{-g} = a^3(t)$ . Substituting this into Eq. (2.6) yields the equations of motion

$$\ddot{\phi} + 3H\dot{\phi} - \frac{1}{a^2(t)} \vec{\nabla}^2 \phi + V(\phi) = 0, \quad (2.10)$$

where  $H = \frac{\dot{a}(t)}{a(t)}$  is the Hubble constant [5] [9]. The slow-roll parameter  $3H\dot{\phi}$  mediates the rate of change of the parameters that describe the field  $\phi$  [8].

The methods described previously enable the study of events taking place in flat spacetime. Physical spacetime exhibits curvature; however, because the curvature is slight, perturbation theory may be utilized to calculate approximate solutions of systems in curved spacetime. By introducing a perturbation to the metric  $\delta g_{\mu\nu}$ , the effects of slight curvature may be introduced to the equations of motion to develop a description of the fields in curved spacetime to linear order. The most general metric perturbation to the FLRW metric is [10]

$$ds^2 = -(1 + 2A)dt^2 + 2\partial_i B dx^i dt + a^2 [(1 - 2\psi)\delta_{ij} + 2\partial_i \partial_j E] dx^i dx^j, \quad (2.11)$$

where  $A$ ,  $B$ ,  $E$ , and  $\psi$  are functions of both space and time that describe the magnitude and structure of the curvature of spacetime. The equations of motion for the field  $\phi$  may then be solved in this perturbed spacetime to determine the evolution of  $\phi$ .

## 2.4 Multi-Field Models of Inflation

Numerous single-field models of inflation exist, and current data lacks the resolution to distinguish between these models. As a result, no single-field inflation model is generally accepted. In addition, due to a lack of a natural limit on the number of inflaton fields that may be present, the existence of multiple inflaton fields cannot be ruled out [10]. Multi-field inflationary models, which assume the existence of multiple distinct inflaton fields, may be analyzed in much the same manner as single-field models [10]. The equations of motion for each of the individual fields  $\phi_q$  from among the set of fields  $\{\phi_q\}$  in the FLRW metric are the same as in Eq. (2.10), assuming that  $\phi$  is replaced by  $\phi_q$  [10]. Note that in this case, each field  $\phi_q$  may be treated independently of the other fields.

Dante’s Inferno is a multi-field model of inflation [1] that assumes the existence of two fields  $r$  and  $\alpha$ . The potential generated by these fields, which appears in Figure 2.2, features a steep-walled “trench” that confines the inflaton field. The spiraling descent of the potential is a property exhibited by spiral inflation models, a class of multi-field inflation models of which Dante’s Inferno is a subset. Spiral inflation models are motivated by axion fields, a class of scalar fields that arise in theories featuring spontaneously broken anomalous symmetries. The field exhibits fluctuations that may occur in any direction; however, the steepness of the walls of the trench prevent significant deviation in the  $\hat{r}$ –direction. The behavior induced by this field is analogous to a ball confined to a wire. A ball thrown in the air is free to move in any direction with no preferential direction, similar to a field existing outside the presence of a Dante’s Inferno potential. However, if the ball is confined to a wire, it exhibits directional preference (along the direction of the wire) and requires extreme amounts of energy to deviate from this path, just as the field requires significant energy to fluctuate in the  $\hat{r}$ –direction. For this reason, the Dante’s Inferno model, along with

other spiral inflation models, can be approximated as single-field models. Though Dante's Inferno may be described using a single-field approximation, it still exhibits potentially desirous properties inherent to certain multi-field models; notably, unlike many single-field models, the Dante's Inferno model predicts high power in gravitational waves. If this class of gravitational wave is detected, numerous single-field models must be discarded, while this model may continue to provide an accurate description of inflation. However, it is also important to rule out large isocurvature fluctuations to correlate predictions of the model with observation [6].

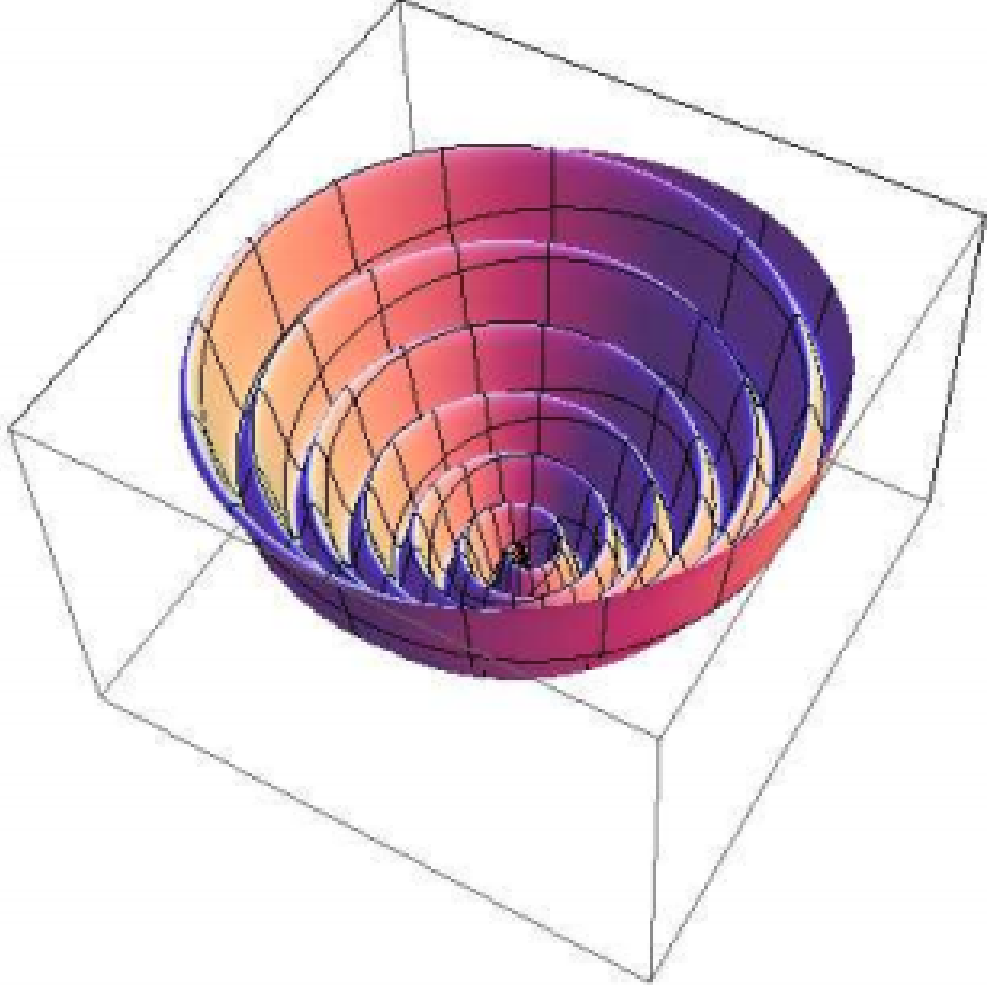


Figure 2.2: The field generated by Dante's Inferno as a function of  $r$  and  $\alpha$ . Note the spiral pattern generated by the steep-walled trench [3].

As predicted by Einstein's theory of general relativity, the presence of energy causes the spacetime around that energy to warp. This energy may be stored within changing fields. Isocurvature fluctuations describe quantum fluctuations of the inflaton field that do not induce a change in spacetime curvature. In spiral inflation models, these fluctuations correspond to fluctuations in the direction of the walls of the trench [2] [3]. Previous studies, such as [2] and [3], have assumed that, due to the steepness of the walls of the trench,

isocurvature fluctuations are negligible; however, an analysis of the size of these fluctuations in certain models has not yet been performed. Therefore, the goal of this project is to perform a detailed study of isocurvature fluctuations in the Dante’s Inferno model of inflation.

## **2.5 Outline**

In the following section, we first demonstrate that isocurvature fluctuations are negligible in single-field models of inflation, then demonstrate that multi-field spiral inflation models may be treated as single-field models, enabling us to apply the single-field results to the multi-field model. We then focus on the Dante’s Inferno model and numerically calculate observables.



# Chapter 3

## Procedure and Results

### 3.1 Single-Field Models of Inflation

The standard Lagrangian for a massive scalar field is

$$\mathcal{L} = \frac{1}{2} \partial_\mu \phi \partial^\mu \phi - \frac{1}{2} m^2 \phi^2. \quad (3.1)$$

By performing a Fourier transform, the equations of motion are obtained:

$$\ddot{\phi}_I + 3H\dot{\phi}_I + \left( \frac{k^2}{a^2} + m^2 \right) \phi_I = 0, \quad (3.2)$$

where  $\phi_I$  is an arbitrary Fourier mode of the field  $\phi$ . The Hubble constant  $H$  is assumed to be constant, providing an accurate approximation assuming the universe expands slowly.

By assuming an ansatz of the form  $\phi(t) = Ae^{\omega t}$ , where  $\omega$  is the temporal frequency of the Fourier modes, Eq. (3.2) reduces to

$$\omega^2 + 3H\omega + \left(\frac{k^2}{a^2} + m^2\right) = 0, \quad (3.3)$$

which is satisfied when

$$\omega = \frac{-3H \pm \sqrt{9H^2 - 4\left(\frac{k^2}{a^2} + m^2\right)}}{2}. \quad (3.4)$$

From Eq. (3.4), it can be seen that when  $\left(\frac{k^2}{a^2} + m^2\right) > \frac{9}{4}H^2$ ,  $\omega$  is complex, so the solutions to Eq. (3.2) are decaying exponential functions that oscillate of the form  $\phi_I = A \exp\left(\left(-\frac{3H}{2} \pm bi\right)t\right)$ , where  $A$  is an arbitrary real number and  $b = \sqrt{\left(\frac{k^2}{a^2} + m^2\right) - \frac{9}{4}H^2}$  is a positive real number. In contrast, if  $\left(\frac{k^2}{a^2} + m^2\right) < \frac{9}{4}H^2$ ,  $\omega$  is real, so the solutions to Eq. (3.2) are of the form  $\phi_I = A \exp\left(\left(-\frac{3H}{2} \pm b\right)t\right)$ . In this case, one solution decays at a slower rate than the oscillatory solutions, so after a long period of time, the solutions in which  $\left(\frac{k^2}{a^2} + m^2\right) > \frac{9}{4}H^2$  become negligibly small when compared to solutions in which  $\left(\frac{k^2}{a^2} + m^2\right) < \frac{9}{4}H^2$ .  $\frac{k}{a}$  is a constant for a given Fourier mode, so in general, if  $m^2 \gg H^2$ , the solutions produced are oscillatory, and therefore die off quickly enough to be negligible compared to the non-oscillatory solutions. Therefore, if  $m^2 \gg H^2$ , the field fluctuations are negligible.

## 3.2 Multi-Field Models of Inflation

In the case of a two-field model of inflation with fields  $\phi$  and  $\chi$ , define a field  $\sigma$  such that [10]

$$\dot{\sigma} = \dot{\phi} \cos \theta + \dot{\chi} \sin \theta, \quad (3.5)$$

where

$$\cos \theta = \frac{\dot{\phi}}{\sqrt{\dot{\phi}^2 + \dot{\chi}^2}} \quad (3.6)$$

and

$$\sin \theta = \frac{\dot{\chi}}{\sqrt{\dot{\phi}^2 + \dot{\chi}^2}}. \quad (3.7)$$

From this definition,  $\theta$  represents the angle of the classical trajectory in field space, and  $\dot{\sigma}$  represents the path length along the classical trajectory. A diagram of the fields in field space may be seen in Figure 3.1. By summing the equations of motion for a single-field model for both  $\phi$  and  $\chi$ , Eq. (2.10), the equations of motion for  $\sigma$  can be derived:

$$\ddot{\sigma} + 3H\dot{\sigma} + V_{\sigma} = 0, \quad (3.8)$$

where

$$V_{\sigma} = V_{\phi} \cos \theta + V_{\chi} \sin \theta \quad (3.9)$$

and  $V_{\beta} = \frac{\partial V}{\partial \beta}$  for an arbitrary field  $\beta$  [10].

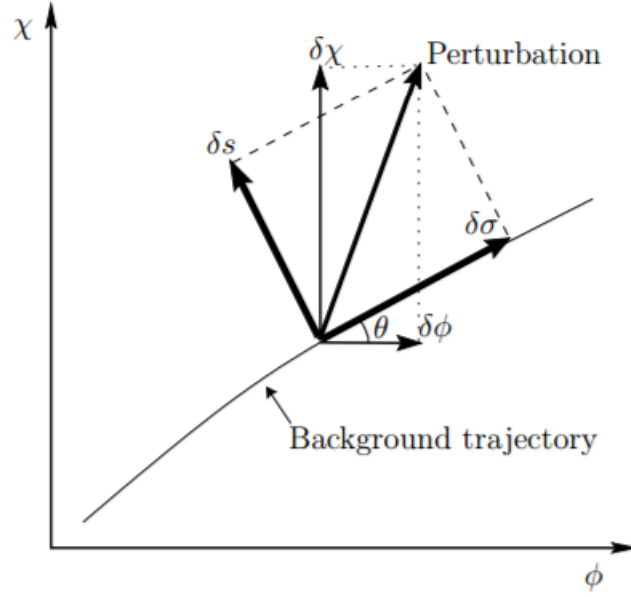


Figure 3.1: The  $\sigma$  and  $s$  fields for an arbitrary perturbation in field space, where the fields are  $\phi$  and  $\chi$ .  $\sigma$  denotes perturbations along the background trajectory,  $s$  denotes perturbations orthogonal to the background trajectory, and  $\theta$  denotes the angle of the background trajectory with respect to  $\phi$  [10].

In addition, a field  $s$  can be defined that is orthogonal to  $\sigma$ :

$$\delta s = \delta \chi \cos \theta - \delta \phi \sin \theta, \quad (3.10)$$

with the corresponding derivative of the potential

$$V_s = V_\chi \cos \theta - V_\phi \sin \theta. \quad (3.11)$$

From these constructions, equations of motion may be derived for  $\delta s$  and  $\delta \sigma$ :

$$\begin{aligned}\ddot{\delta\sigma} + 3H\dot{\delta\sigma} + \left(\frac{k^2}{a^2} + V_{\sigma\sigma} - \dot{\theta}^2\right)\delta\sigma = \\ = -2V_{\sigma A} + \dot{\sigma}\left[\dot{A} + 3\dot{\psi} + \frac{k^2}{a^2}\left(a^2\dot{E} - aB\right)\right] + 2(\dot{\theta}\delta s) - 2\frac{V_{\sigma}}{\dot{\sigma}}\dot{\theta}\delta s\end{aligned}\quad (3.12)$$

and

$$\ddot{\delta s} + 3H\dot{\delta s} + \left(\frac{k^2}{a^2} + V_{ss} - \dot{\theta}^2\right)\delta s = -2\frac{\dot{\theta}}{\dot{\sigma}}\left[\dot{\sigma}\left(\dot{\delta\sigma} - \dot{\sigma}A\right) - \ddot{\sigma}\delta\sigma\right], \quad (3.13)$$

where

$$V_{\sigma\sigma} = V_{\phi\phi}\cos^2\theta + 2V_{\phi\chi}\cos\theta\sin\theta + V_{\chi\chi}\sin^2\theta, \quad (3.14)$$

$$V_{ss} = V_{\chi\chi}\cos^2\theta - 2V_{\phi\chi}\cos\theta\sin\theta + V_{\phi\phi}\sin^2\theta, \quad (3.15)$$

$$\dot{\theta} = -\frac{V_s}{\dot{\sigma}}, \quad (3.16)$$

and  $A$ ,  $E$ , and  $\psi$  correspond to those variables seen in Eq. (2.11) [10]. The comoving matter perturbation  $\varepsilon_m$  may be defined as

$$\varepsilon_m = 2\dot{\sigma}\dot{\theta}\delta s + \dot{\sigma}(\dot{\delta\sigma} - \dot{\sigma}A) - \ddot{\sigma}\delta\sigma, \quad (3.17)$$

and substituting this into Eq. (3.13) yields [10]:

$$\varepsilon_m = \ddot{\delta s} + 3H\dot{\delta s} + \left(\frac{k^2}{a^2} + V_{ss} - 3\dot{\theta}^2\right)\delta s. \quad (3.18)$$

Over large scales,  $\varepsilon_m$  is negligible, so Eq. (3.18) becomes

$$\ddot{\delta s} + 3H\dot{\delta s} + \left( \frac{k^2}{a^2} + V_{ss} - 3\dot{\theta}^2 \right) \delta s = 0. \quad (3.19)$$

Each term on the right-hand side of Eq. (3.19) depends on  $\delta s$  and its derivatives. Thus, if  $\delta s$  initially is zero, then over large scales, it will remain zero [10].

### 3.3 Dante's Inferno

The Dante's Inferno model of inflation assumes the existence of the inflaton fields  $r$  and  $\alpha$ , which produce a potential of the form [1] [2] [3]

$$V(r, \alpha) = W(r) + \Lambda^4 \left( 1 - \cos \left( \frac{r}{f_r} - \frac{\alpha}{f_\alpha} \right) \right), \quad (3.20)$$

where  $W(r)$  is an arbitrary function and  $\Lambda$ ,  $f_r$ , and  $f_\alpha$  are constants. Due to the  $\cos \left( \frac{r}{f_r} - \frac{\alpha}{f_\alpha} \right)$  term, the potential is semi-periodic, so it is natural to consider this potential in cylindrical coordinates in field space, where  $r$  corresponds to the radial coordinate and  $\alpha$  corresponds to the angular coordinate. In the case  $W(r) = \frac{1}{2}m^2 r^2$ , where  $m$  is the mass of the  $r$ -field, the potential is of the form [1] [2] [3]

$$V(r, \alpha) = \frac{1}{2}m^2 r^2 + \Lambda^4 \left( 1 - \cos \left( \frac{r}{f_r} - \frac{\alpha}{f_\alpha} \right) \right), \quad (3.21)$$

and is displayed in Figure 2.2.

In the Dante's Inferno model of inflation, the isocurvature fluctuations are negligible due to the structure of the trench; however, it is not immediately obvious which field represents the isocurvature field. The classical trajectory of the field roughly follows the bottom of

the trench, and is primarily in the  $\hat{\alpha}$ –direction. By construction, the  $s$ –field corresponds to field oscillations normal to the classical trajectory; thus, the  $s$ –field is dominated by the  $r$ –field. The comoving curvature perturbation  $\mathcal{R}$ , or total curvature perturbation in comoving coordinates, is defined as [10]

$$\mathcal{R} = \psi + \frac{H}{\dot{\sigma}} \delta\sigma, \quad (3.22)$$

but may be decomposed in terms of  $\mathcal{R}_\alpha$  and  $\mathcal{R}_r$ , the comoving curvature perturbation induced by the  $\alpha$ - and  $r$ -fields, respectively as

$$\mathcal{R} = \mathcal{R}_\alpha \cos^2 \theta + \mathcal{R}_r \sin^2 \theta. \quad (3.23)$$

As the classical trajectory nearly coincides with the  $\alpha$ –direction,  $\theta \ll 1$ , so  $\sin \theta \approx \theta$  and  $\cos \theta \approx 1 - \theta^2$ . To first order,  $\sin^2 \theta \approx 0$  and  $\cos^2 \theta \approx 1$ , indicating that  $\mathcal{R} \approx \mathcal{R}_\alpha$ . Thus, to first order, the comoving curvature perturbation is composed entirely of the perturbation in the  $\alpha$ –direction, so spacetime curvature is primarily induced by the  $\alpha$ -field. As the isocurvature field does not contribute to the comoving curvature perturbation, the adiabatic field must be dominated by  $\alpha$ . The adiabatic field is orthogonal to the isocurvature field in field space, so  $r$  must dominate the isocurvature field, indicating that the perturbations in the  $r$ –direction correspond to isocurvature perturbations.

### 3.3.1 Numerical Results

In the Dante's Inferno model, the fields  $r$  and  $\alpha$  have effective masses which may be described by the mass matrix  $\mathcal{M}$ :

$$\mathcal{M} = \begin{pmatrix} \frac{\partial^2 V}{\partial r^2} & \frac{\partial^2 V}{\partial r \partial \alpha} \\ \frac{\partial^2 V}{\partial r \partial \alpha} & \frac{\partial^2 V}{\partial \alpha^2} \end{pmatrix}. \quad (3.24)$$

The fluctuations in the  $\hat{r}$ -direction are suppressed, indicating that the field will remain near the minimum of the trench throughout its trajectory. As the minimum of the trench is defined as the location at which  $\frac{dV}{dr} = 0$ , the off-diagonal components of Eq. (3.24) will be negligible, diagonalizing the mass matrix. This indicates that the interactions between  $r$  and  $\alpha$  will be negligible, so each field may be treated independently, enabling the single-field approximation to be used for each. As demonstrated in Section 3.1, the isocurvature fluctuations may be ignored if  $\frac{k^2}{a^2} + m^2 > \frac{9}{4}H^2$ , a condition that is met if  $m^2 > \frac{9}{4}H^2$ . Thus, to determine whether isocurvature fluctuations are negligible, it must be shown that  $\frac{d^2 V}{dr^2} > \frac{9}{4}H^2$ .

As demonstrated in [1], appropriate values for  $m$ ,  $f_r$ ,  $f_\alpha$ , and  $\Lambda$  are  $m = 10^{-4}M_p$ ,  $f_r = 10^{-3}M_p$ ,  $f_\alpha = 10^{-1}M_p$ , and  $\Lambda = 10^{-3}M_p$ . To calculate the mass of the inflaton field, the potential along the minimum of the trench was parameterized in terms of  $\alpha$  so that  $V(r, \alpha) \rightarrow V(R(\alpha), \alpha)$ , where  $R(\alpha)$  represents the  $r$ -field coordinate along the minimum of the trench. The slow roll parameter  $\varepsilon$ , which is defined as [2] [3] [11]

$$\varepsilon = \frac{M_p^2}{16\pi} \left( \frac{dV}{d\alpha} / V \right)^2, \quad (3.25)$$



was calculated. Inflation ends at  $\alpha = \alpha_f$ , where  $\varepsilon_f = \varepsilon(\alpha = \alpha_f) = 1$ , and begins at  $\alpha = \alpha_i$ , where  $\alpha_i$  is defined as the  $\alpha$  coordinate such that the number of e-folds  $N_e$ , or the number of times the radius of the universe increased by a factor of  $e$  during inflation, corresponds with what is observed in the CMB. It has been found that  $N_e(\alpha_f) - N_e(\alpha_i) = 60$ , which corresponds to an increase in radius by a factor of  $10^{26}$  [6]. The number of e-folds may be calculated using [2] [3] [11]

$$N_e(\alpha_f) - N_e(\alpha_i) = \int_{\alpha_i}^{\alpha_f} \frac{2\sqrt{\pi}}{M_p \sqrt{\varepsilon}} d\alpha. \quad (3.26)$$

Though this cannot be calculated analytically, it may be approximated: as  $\Lambda^4$  is small in comparison with the other terms in the potential, Eq. (3.21), and  $|1 - \cos(\frac{r}{f_r} - \frac{\alpha}{f_\alpha})| \leq 1$ ,  $\Lambda^4(1 - \cos(\frac{r}{f_r} - \frac{\alpha}{f_\alpha}))$  is negligible. In this approximation,  $V(R(\alpha), \alpha) \approx \frac{1}{2}m^2 r^2$ . At the minimum of the trench,  $\cos(\frac{r}{f_r} - \frac{\alpha}{f_\alpha}) = 1$ , so

$$r = \frac{f_r}{f_\alpha} \alpha. \quad (3.27)$$

Thus,

$$V(R(\alpha), \alpha) \approx \frac{1}{2}m^2 \left( \frac{f_r}{f_\alpha} \alpha \right)^2. \quad (3.28)$$

Using Eq. (3.25) and Eq. (3.28), the functional form of  $\varepsilon$  may be approximated as

$$\varepsilon = \frac{M_p^2}{4\pi} \frac{1}{\alpha^2}, \quad (3.29)$$

and the location  $\alpha_f$  such that  $\varepsilon_f = \varepsilon(\alpha_f) = 1$  may be found analytically to be  $\alpha_f = \frac{1}{2\sqrt{\pi}}$ .

The location  $\alpha_i$  at which inflation began may be found using Eq. (3.26) to be  $\alpha_i = \frac{11}{2\sqrt{\pi}}$ ,

as  $N_e(\alpha_f) - N_e(\alpha_i) = 60$ . Similarly, the slow roll parameter  $\eta$  may be defined as [2] [3] [11]

$$\eta = \frac{M_p^2}{8\pi} \frac{d^2 V}{d\alpha^2} \bigg/ V. \quad (3.30)$$

This parameter describes the curvature of the potential, and like  $\varepsilon$  may be approximated as

$$\eta = \frac{M_p^2}{4\pi} \frac{1}{\alpha^2}. \quad (3.31)$$

Using these definitions, the scalar tilt  $n_s = 1 + 2\eta_i - 6\varepsilon_i$  may be approximated as  $n_s \approx \frac{116M_p^2}{121} \approx 0.959M_p^2$ . Numerically calculating  $n_s$  yields  $n_s = 0.966M_p^2$ , and both of these results agree with [2] and the data from the Planck collaboration located in [6]. In addition, the scalar-to-tensor ratio,  $\tilde{r} = 16\varepsilon_i$  may be approximated as  $\tilde{r} \approx \frac{16M_p^2}{121} \approx 0.132M_p^2$ . Similarly, numerical results yield  $\tilde{r} = 0.132M_p^2$ , which is in agreement with  $\tilde{r} = 0.14M_p^2$  as reported in [1].

Next, the trajectory of  $r$  and  $\alpha$  in field space was found. The equations of motion for  $r(t)$  and  $\alpha(t)$  are

$$\ddot{r}(t) + 3H\dot{r}(t) + \frac{dV}{dr} = 0 \quad (3.32)$$

and

$$\ddot{\alpha}(t) + 3H\dot{\alpha}(t) + \frac{dV}{d\alpha} = 0, \quad (3.33)$$

where

$$H^2 = \frac{8\pi G}{3} \left( V(r(t), \alpha(t)) + \frac{1}{2} \dot{r}(t)^2 + \frac{1}{2} \dot{\alpha}(t)^2 \right). \quad (3.34)$$

Using Eq. (3.27), this may be rewritten as

$$H^2 = \frac{8\pi G}{3} \left( V(r(t), \alpha(t)) + \frac{1}{2} \left( 1 + \frac{f_r^2}{f_\alpha^2} \right) \dot{\alpha}(t)^2 \right). \quad (3.35)$$

Solving Eq. (3.32) and Eq. (3.33) numerically provides a parameterization of the trajectory of the field in field space, which may be seen in Figure 3.2. In addition, using Eq. (3.33) and Eq. (3.35),  $\frac{d^2 V}{dr^2}$  may be found numerically. This quantity represents the effective mass of the isocurvature field. As the mass matrix  $\mathcal{M}$  in Eq. (3.24) is diagonal, the isocurvature field may be treated independently from the adiabatic field, allowing the results of the single-field case to be utilized: if  $\frac{d^2 V}{dr^2} > \frac{9}{4} H^2$ , or  $\frac{d^2 V}{dr^2} / \frac{9}{4} H^2 > 1$ , then the isocurvature fluctuations are suppressed. As may be seen in Figure 3.3, this condition is upheld numerically, demonstrating that the isocurvature fluctuations will be suppressed in the Dante's Inferno model of inflation.

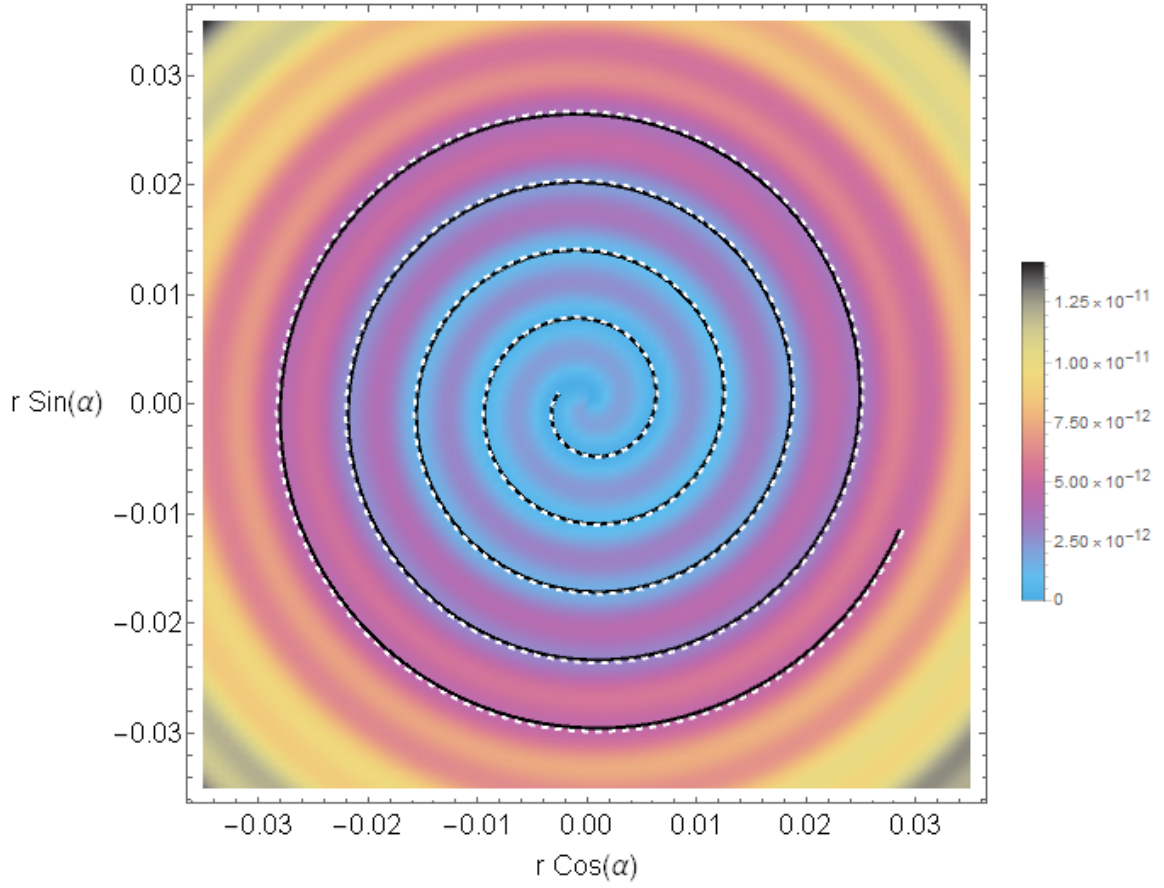


Figure 3.2: A display of the trajectory of the inflaton field. The colored background is a density plot of the potential in polar coordinates evaluated in Planck units, the solid black line represents the minimum of the trench, and the dashed white line represents the trajectory of the field with initial conditions  $\alpha(t = t_i) = \alpha_i + 10^{-5}$  and  $\dot{\alpha}(t = t_i) = -10^{-8}$ . These conditions correspond to the initial conditions at the beginning of inflation with a slight angular deviation and initial velocity. Both the solid black line and dashed white line begin on the outside of the spiral and end near the center.

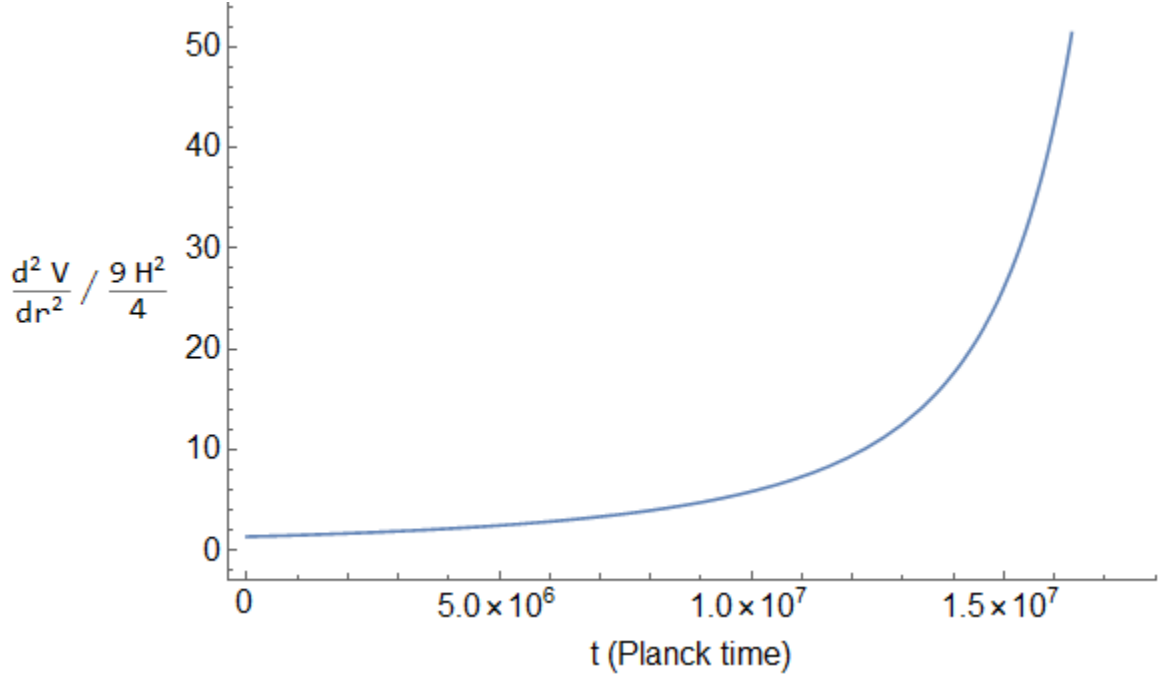


Figure 3.3: A display of the ratio of the isocurvature field mass to  $\frac{9}{4}H^2$ . As the ratio is always greater than unity, the field mass is large enough to suppress entropic fluctuations. As time increases, the value of the ratio decreases, indicating that around the time that inflation ends, the isocurvature fluctuations become non-negligible. Though isocurvature fluctuations are not observed in the cosmic microwave background, this does not rule out Dante’s Inferno, as the isocurvature fluctuations generated near the beginning of inflation would have a frequency larger than is currently observable.

### 3.4 Conclusions and Future Plans

In this project, we were successful in demonstrating that low-mass fluctuations dominate over their high-mass counterparts in single-field inflation, and that the isocurvature fluctuations are negligible in comparison to the adiabatic fluctuations in the Dante’s Inferno model. We analytically demonstrated that high-mass fluctuations are negligible in single-field inflation, then proved that the  $r$ – and  $\alpha$ –fields in Dante’s Inferno may be treated independently of one another by diagonalizing the mass matrix. We applied the single-field inflation results to Dante’s Inferno to demonstrate that radial fluctuations cor-

respond to isocurvature modes and are suppressed. Numerical methods were used to verify these results: we solved the equations of motion to determine the trajectory of the inflation field in field space and demonstrated that the field remains near the minimum of the trench. In addition, it was found that  $m_r^2 > \frac{9}{4}H^2$  during the entirety of inflation, indicating that isocurvature fluctuations are suppressed during this time; however, near the beginning of the period, the fluctuations are not heavily suppressed, indicating that there may exist high-frequency isocurvature fluctuations from inflation that have not yet been observed. Numerical methods also demonstrated that the Dante’s Inferno model predicts a scalar tilt and scalar-to-tensor ratio that match observational evidence, indicating that Dante’s Inferno provides a realistic description of inflation. Future work could be dedicated to understanding the implications of the Dante’s Inferno model in the time period following inflation, such as the behavior of the field when the field reaches the global minimum of the potential. In addition, the results may be used to calculate the correlation functions and other inflationary observables that would be expected from the parameters used in the model to determine whether Dante’s Inferno accurately describes the observed quantities.

# Bibliography

- [1] Marcus Berg, Enrico Pajer, and Stefan Sjors. “Dante’s Inferno”. In: *Phys. Rev. D* 81 (2010), p. 103535. eprint: [0912.1341](#).
- [2] Joshua Erlich, Jackson Olsen, and Zhen Wang. “The field-space metric in spiral inflation and related models”. In: *JCAP* 1609.09 (2016), p. 039. eprint: [1509.06781](#).
- [3] Christopher D. Carone et al. “Two-field axion-monodromy hybrid inflation model: Dante’s Waterfall”. In: *Phys. Rev. D* 91.4 (2015), p. 043512. eprint: [1410.2593](#).
- [4] Bernard Schutz. *A First Course in General Relativity*. 1985.
- [5] David H. Lyth and Andrew R. Liddle. *The primordial density perturbation: Cosmology, inflation and the origin of structure*. 2009.
- [6] P. A. R. Ade et al. “Planck 2015 results. XX. Constraints on inflation”. In: *Astron. Astrophys.* 594 (2016), A20. eprint: [1502.02114](#).
- [7] N. Aghanim et al. “Planck 2015 results. XI. CMB power spectra, likelihoods, and robustness of parameters”. In: *Astron. Astrophys.* 594 (2016), A11. eprint: [1507.02704](#).
- [8] Shinji Tsujikawa et al. “Planck constraints on single-field inflation”. In: *Phys. Rev. D* 88.2 (2013), p. 023529. eprint: [1305.3044](#).
- [9] Xingang Chen et al. “Observational signatures and non-Gaussianities of general single field inflation”. In: *JCAP* 0701 (2007), p. 002. eprint: [hep-th/0605045](#).
- [10] Christopher Gordon et al. “Adiabatic and entropy perturbations from inflation”. In: *Phys. Rev. D* 63 (2001), p. 023506. eprint: [astro-ph/0009131](#).
- [11] Christopher D. Carone et al. “Permutation on hybrid natural inflation”. In: *Phys. Rev. D* 90.6 (2014), p. 063521. eprint: [1407.6017](#).